Radiation Physics and Chemistry 173 (2020) 108871

Contents lists available at ScienceDirect

Radiation Physics and Chemistry

journal homepage: www.elsevier.com/locate/radphyschem

Radiocatalytic performance of oxide-based nanoparticles for targeted therapy and water remediation

M. Molina Higgins (Ph.D)[a], A. Banu (Ph.D)[b], S. Pendleton (Ph.D)[b], J.V. Rojas (Ph.D)[a,*]

[a] Department of Mechanical and Nuclear Engineering, Virginia Commonwealth University, Richmond, United States
[b] Department of Physics and Astronomy, James Madison University, Harrisonburg, VA, United States

ARTICLE INFO

Keywords:
Radiocatalysis
X-rays
Methylene blue
Supported gold nanoparticles
Metal oxide nanoparticles

ABSTRACT

The radiocatalytic behavior of zinc oxide (ZnO), hafnia (HfO_2), titania (TiO_2), and gold-titania (Au@TiO_2) nanomaterials was investigated through the degradation of methylene blue as the organic probe. The dye degradation by X-rays from a medical linear accelerator with endpoint energy of 6 MeV was enhanced in the presence of the oxide-based nanoparticles evidencing their promise as radiosensitizers. An increase in the dye apparent reaction rate constants of ~20% and up to 82% was observed in the presence of oxides-based nanoparticles during exposure to X-rays. This enhancement is attributed to the increased production of reactive species in solution. Gold-titania nanocomposites evidenced one of the highest radiocatalytic activity among the materials under investigation, with an increase in the MB apparent reaction rate constant of 50.3%. Overall, our experiments showed that radiocatalysis with oxides-based nanoparticles is a promising concept worth exploring in applications such as targeted radiation therapy and pollutant removal of water streams.

1. Introduction

Along with all the revolutionary discoveries in nanotechnology, metal oxides nanostructures have unveiled their superior catalytic performance, and their use has been explored in different industries such as medical, pharmaceutical, oil refining, energy storage, food, cosmetics, and environmental remediation (Védrine, 2017). Metal oxides are wide bandgap semiconductors, naturally abundant, with low toxicity to living organisms, and chemically stable (Chen and Wang, 2014). They have shown outstanding promises on catalytic processes that take advantage of the production of reactive oxygen species (ROS), such as superoxide radicals ($O_2^{\bullet-}$) and hydroxyl radicals ($OH^{\bullet}$), to decompose unwanted chemical and biological agents. These processes include ozonation, photo- and radio-catalysis, low-temperature plasma, and Fenton processes. (Cheng et al., 2016; Rauf and Ashraf, 2009). Among the different novel alternatives for water decontamination, those that rely on the use of radiation have shown promise. Specifically, radiocatalysis is a phenomenon characterized by the interaction of a catalyst with ionizing radiation to increase the rate of a chemical reaction. (Hoertz et al., 2013; Sahu and Cates, 2017; Samet et al., 2018). The accelerated degradation of pollutants under ionizing radiation has been explained based on their interaction with radicals that result from the radiolysis of water (Appleby and Schwarz, 1969; Hamill, 1969; Rauf and Ashraf, 2009). Herein, water molecules dissociate into reactive species such as aqueous electrons (e^-_{aq}), hydrogen atoms ($H^{\bullet}$), hydrogen molecules (H_2), hydrogen peroxide (H_2O_2), and hydroxyl radicals ($OH^{\bullet}$) (Hamill, 1969; LaVerne, 2000). These species interact with the contaminants, in a process that involves the conversion of pollutants into smaller compounds (Guo, 2018; Rauf and Ashraf, 2009). Studies on radiocatalysis have shown that the combination of metal oxide semiconductors nanoparticles (NPs) with ionizing radiation may provide faster results than conventional methods in photocatalysis, which uses visible or UV light (Samet et al., 2018). Besides the radiolysis of water, ionizing radiation such as X-rays and gamma rays also generates a higher density of electron-hole pairs in semiconductors as compared to UV light. Furthermore, the penetration depth of X-rays and gamma-rays is significantly higher than that of visible/UV light, which allows for processing large volumes of contaminated water. All the aforementioned phenomena combine into radiocatalysis to increase the decomposition rate of targeted biological and chemical compounds (Guo, 2018; Rauf and Ashraf, 2009). In environmental applications, the concept of radiocatalysis has been explored for soil and groundwater remediation. As such, Cobalt-60 rods in conjunction with Al_2O_3 NPs have been used to reduce toxic substances present in both soil and water (Zacheis et al., 1999; Sahu and Cates, 2017).

The catalytic properties of metal oxide semiconductor nanoparticles have also been studied in the medical field (Sahu and Cates, 2017; Stafford et al., 1994; Yin et al., 2013). For instance, titania (TiO_2) and

* Corresponding author.
E-mail addresses: molinahiggimc@vcu.edu (M. Molina Higgins), banula@jmu.edu (A. Banu), pendlesj@jmu.edu (S. Pendleton), jvrojas@vcu.edu (J.V. Rojas).

https://doi.org/10.1016/j.radphyschem.2020.108871
Received 3 May 2019; Received in revised form 30 January 2020; Accepted 15 March 2020
Available online 18 March 2020
0969-806X/

Zinc Oxide (ZnO) have been explored as sensitizing agents in photodynamic therapy (PDT), a methodology that uses chemical compounds in combination with a visible or UV light source to destroy cancer cells (Yin et al., 2013). In this technique, the interaction of light with the photosensitizer leads to the creation of reactive oxygen species (ROS) that destroy malignant cells (Yin et al., 2013). Nonetheless, PDT is only used to treat superficial tumors due to the low penetration of visible and UV light in tissue (Kotagiri et al., 2015). The implementation of metal oxides to treat internal tumors could benefit from the use of radiation with a higher penetration depth such as X-rays, gamma rays, and high-energy electron beams due to their low linear energy transfer (LET). The combined use of chemical compounds and ionizing radiation to treat tumors is a technique known as radiosensitization (Wang et al., 2018). In practice, radiosensitizers may be directed into malignant tumors and irradiated using an external beam (Tourneau et al., 2018; Youkhana et al., 2017). Results have shown that certain nanoparticles cause a localized increase of the mass-energy absorption coefficient, accelerating the damage to carcinogenic cells and tumors (Generalov et al., 2015; Sahu and Cates, 2017; Youkhana et al., 2017; Zhou et al., 2019). In recent years, nanomaterials composed of elements with high atomic numbers have been explored as radiosensitizers due to their ability to absorb high energy photons and emit secondary radiation (Wang et al., 2018). Some of the nanomaterials that have been explored as radiosensitizers include those containing bismuth (Bi), tungsten (W), hafnium (Hf), iron (Fe), gadolinium (Gd), and gold (Au) (Hainfeld et al., 2004; Kuncic and Lacombe, 2018; Maggiorella et al., 2012; Mesbahi, 2010; Rajaee et al., 2019; Zhou et al., 2019). As an example, Nanoclusters of BiP_5W_{30} have shown an increased energy deposition within HeLa tumors and cells (Zhou et al., 2019). Also, $BiGdO_3$ nanoparticles have been studied as radiosensitizers by gel dosimetry, in-vitro, and in-vivo experiments, evidencing dose rate amplification and promise as contrast agents for imaging purposes (Rajaee et al., 2019). Au nanoparticles with size ranging from ~2 nm to ~50 nm have been heavily studied as radiosensitizers, and the results indicate that Au nanoparticles produce a high radiosensitization effect in tumor cells and murine tumors (Her et al., 2017).

This work focuses on the novel approach of radiocatalysis with wide bandgap semiconductors. Herein, TiO_2, Au@TiO_2, ZnO, and HfO_2 are activated using X-rays, and their radiocatalytic performance is evaluated by monitoring their effects on the degradation of methylene blue (MB). TiO_2 NPs are currently studied in diverse environmental applications such as water splitting, production of hydrocarbons, pollutant and bacteria removal from air and water, as well as in medical applications e.g. cancer therapy (Nakata and Fujishima, 2012; Yin et al., 2013). With TiO_2 being a wide bandgap semiconductor (~3.2 eV), deposition of high atomic number (Z) metals such as gold (Au) is used to reduce the recombination rate of electron-hole pairs and its bandgap (Primo et al., 2011). Furthermore, ZnO is a semiconductor used in different electronic applications such as ferromagnetism, optoelectronics, transducers technology, and solar cell harvesting (Banerjee, 2017; Beek et al., 2004; Djurišić et al., 2010; Gao et al., 2009). ZnO has a bandgap of ~3.3 eV, and relevant characteristics for catalysis include mild to low toxicity, corrosion resistance, and environmental sustainability (Banerjee, 2017). Finally, HfO_2 has a high melting point (~2700 °C), high dielectric constant, and a bandgap of ~5 eV. Nanoparticles of HfO_2 have been used for electronic and radiation therapy applications (Tourneau et al., 2018; Wan and Zhou, 2017).

Our previous work in this topic has reported a detailed synthesis route for Au@TiO_2 nanocomposites as well as the dose enhancement response upon interaction with X-rays using chemical dosimeters and bacteria cells. In these studies, the dose enhancement phenomenon was evidenced at beam energies in the orthovoltage range (E_{photon} < 500 KeV) (Molina Higgins and Rojas, 2019). While successful results have been obtained, the energies at which such materials where evaluated may restrict their potential use in current therapeutic practices. Nowadays, most of the devices used for external radiation therapy are X-ray machines equipped with linear accelerators that generate photons with energies between 1 and 20 MeV. High energy X-rays can penetrate more deeply in the body, allowing for the targeting of internal tissues while minimizing the energy deposition in the skin and surrounding healthy cells. Thus, this work investigates the radiation enhancement behavior of various oxide-based nanomaterials when exposed to X-rays at the megavoltage range. The results presented in this work is built upon our previous findings and showed the potential of oxides-based nanomaterials to increase the absorbed dose in aqueous environments, which could bring significant progress in both medical and catalysis fields.

2. Experimental procedure

2.1. Materials and reagents

Powders of oxide NPs were acquired from various sources. As such, TiO_2, with the anatase crystal form, was obtained from Nanostructured & Amorphous materials, Inc, having distinct mean particle sizes of 6.5 nm and 21.6 nm and purity greater than 99.0%. Both HfO_2 and ZnO, with a mean particle size of 75 nm and 25.7 nm, were purchased from US Research nanomaterials Inc. Finally, sub-10 nm HfO_2 NPs were synthesized using Hafnium tetrachloride ($HfCl_4$) from Acros Organics and sodium hydroxide (NaOH) obtained from Sigma-Aldrich. Gold (III) chloride trihydrate ($HAuCl_4 \cdot 3H_2O$, ≥99.9% trace metal basis) and isopropanol (C_3H_8O, ≥99.7%), also from Sigma Aldrich, were used in the synthesis of Au@TiO_2. Ultrapure water (18 MΩ) from a Millipore Direct QTM 3 UV purification system was used throughout the experiments.

2.2. Radiolytic synthesis of Au supported TiO_2 nanocomposites

The synthesis through X-rays of Au NPs supported TiO_2 is explained in detail elsewhere (Molina Higgins et al., 2018). Briefly, TiO_2 was added to a 2 mM $HAuCl_4$, whose pH had been adjusted to a value of 8, in a formulation that led to nominal Au loading onto the TiO_2 of 10 wt %. After homogenizing the mixture using an ultrasonic probe, the pH was monitored and adjusted again to ~8 using a concentrated solution of 1 M NaOH. The sample was stirred continuously for 1 h while kept at 80 °C. Afterward, the precipitate was collected by centrifugation and washed a few times to remove unreacted species. The subsequent irradiation step was performed in a Precision X-RAY X-RAD 225 XL irradiator, with W target, at an output voltage of 225 kV and a power of 3000 W. The aqueous suspensions were irradiated at a dose rate of 127 Gy/min until a total absorbed dose of 7.26 kGy was attained. Prior to irradiation, isopropanol in a 10 v/v% was added to scavenge the oxidizing species produced in the radiolysis of water. The materials were identified as $TiO_2^{6.5\ nm}$, $TiO_2^{21.6\ nm}$, Au@$TiO_2^{6.5\ nm}$, and Au@$TiO_2^{21.6\ nm}$.

2.3. Hydrothermal synthesis of HfO_2

Synthesis of HfO_2 with a mean particle size of 8.4 nm, was carried out following a hydrothermal route (Jayaraman et al., 2014). A stock solution (25 ml) of $HfCl_4$ was prepared in a 0.1 M concentration. Then, 25 ml of NaOH solution (0.4 M) was added dropwise to the $HfCl_4$ stock solution. Next, the solution was stirred for 6 h, where a white precipitate of hafnium hydroxide was produced. This precipitate was centrifuged and washed with DI water, dried in an oven at 100 °C for 3 h and calcined at 500 °C for 2 h. The white product was collected and ground to a fine powder. To differentiate the samples of HfO_2 having a different particle size, they were identified as $HfO_2^{8.4\ nm}$ and $HfO_2^{75\ nm}$.

2.4. Characterization of oxide-based nanoparticles

Transmission electron microscopy (TEM) analysis of TiO_2, Au

supported on TiO_2, ZnO, and HfO_2 was performed using a Zeiss Libra 120 plus microscope operated at 120 kV. For this purpose, the nanomaterial was dispersed in acetone, and a drop of the suspension was deposited onto a copper grid. The size of individual particles was measured by using the image processing software Image J 1.5i. X-ray diffraction analysis of the oxide-based NPs was performed in a PAnalytical X'Pert diffractometer with a Cu target set at a voltage and current of 45 kV and 40 mA. To obtain the XRD patterns, the nanomaterial in powder form was placed onto a silicon wafer and then loaded onto the spinning sample stage. The diffraction patterns were analyzed with the software X'pert Highscore. The point of zero charge (pzc) of the supports was measured using a NanoPlus HD zeta analyzer from Micromeritics. For this purpose, the nanomaterials were dispersed in DI water and their pH was modified using NaOH (0.1 M) and HCl (0.1 M), then the zeta potential values were recorded.

2.5. Radiocatalysis assessment of oxide-based semiconductors

Initially, concentrations of 0.2–1 mg/ml were added to aqueous solutions 50 μM of MB. Then, 1 ml of the suspensions was transferred to conical-shaped polypropylene microcentrifuge vials of 1.5 ml volume capacity. It is important to highlight that the MB solutions were air-saturated to avoid reversible degradation processes (Kovács et al., 1998). The pH values of the samples were taken before irradiation for solutions with a concentration of 0.2 mg/ml, giving 6.4 for MB, 4.1 for $TiO_2^{6.5\ nm}$, 6.1 for $TiO_2^{21.6\ nm}$, 4.5 for $Au@TiO_2^{6.5\ nm}$, 6.3 for $Au@TiO_2^{21.6\ nm}$, 7.6 for ZnO, 6.5 for $HfO_2^{8.4\ nm}$ and, 7.0 for HfO_2^{75nm}. Three replicates of each suspension containing the different nanomaterials were prepared and irradiated. The irradiation was conducted in the Madison accelerator laboratory (MAL) at James Madison University, using a LINAC operating in X-ray mode with endpoint energy of 6 MeV and a dose rate of 8 Gy/min, and irradiation field set to 10 × 10 cm. The absorbance of MB at 664 nm was recorded after every 2 min of irradiation up to a total irradiation time of 8 min, and it was used to calculate its corresponding apparent reaction rate constant. The UV-vis patterns were collected with a Genesis 10 S UV-Vis spectrophotometer using quartz cuvettes of 10 mm path length.

3. Results and discussion

3.1. Morphology and crystalline structure of radiosensitizers

The XRD patterns are shown in Fig. 1 for TiO_2, HfO_2, and ZnO revealed their anatase (JCSPDS 01-075-2552), monoclinic (JCSPDS 06-0318) and wurtzite (JCPDS 5-0664) crystal structures, respectively. Moreover, the Au NPs deposited on TiO_2 evidenced its characteristic face-centered cubic structure (JCSPDS 01-071-4614). The crystallite size of the semiconductors was calculated using Scherrer equation and values of 7.1 nm, 18.6 nm, 8.3 nm, 13.1 nm, and 23.5 nm were obtained for $TiO_2^{(6.5\ nm)}$, $TiO_2^{(21.6\ nm)}$, $HfO_2^{(8.4\ nm)}$, $HfO_2^{(75\ nm)}$, and ZnO respectively.

TEM images of the metal oxides are shown in Fig. 2. Statistical analysis of the particle size indicated a mean particle size of 6.5 ± 1.2 nm and 21.6 ± 5.4 nm for TiO_2, 25.7 ± 9.0 nm for ZnO, and 8.4 ± 2.0 nm and 75 ± 18.3 nm for HfO_2. Interestingly, a comparison of the mean particle size of $HfO_2^{(75\ nm)}$ obtained by TEM with the crystallite size obtained by XRD (13.1 nm) evidenced the polycrystalline nature of the particles. The Au NPs onto the TiO_2 as supports were fabricated using X-ray synthesis, a clean fabrication method carried out at NTP conditions (i.e. atmospheric pressure and temperature). The Au particles were found uniformly dispersed on the supports and displayed a mean particle size of ~1.0 ± 0.3 nm. Moreover, chemical analysis of the $Au@TiO_2$ samples with energy dispersive X-ray spectroscopy (EDS) revealed a gold content wt% of 8.4% for $Au@TiO_2^{6.5\ nm}$ and 8.91% for $Au@TiO_2^{21.6\ nm}$. One of the main advantages of radiolytic synthesis is the purity of the product, this feature is of particular importance since an excess of chemicals on the surface of NPs could hinder their catalytic activity (Niu and Li, 2014). Ionizing radiation interacting with water produces a large number of reducing species, such as $H^{\bullet}$ atoms and hydrated electrons (Belloni et al., 1998). Hence, the radiolytic synthesis of supported Au nanoparticles is based on the interaction of these reducing species with the Au cations within the aqueous solution, reducing them to a zero valence through multistep reactions (Belloni et al., 1998; Clifford et al., 2017; Čubová and Čuba, 2019). The atoms within the solution will coalesce and form nucleation centers, followed by NP growth (Belloni et al., 1998; Clifford et al., 2017). Characteristics such as the size and shape of the Au NP depend on the absorbed dose and dose rate used during the synthesis process. A detailed study of the synthesis of Au NPs on TiO_2 using X-rays is described in detail in our previous work (Molina Higgins et al., 2018).

3.2. Radiocatalytic degradation of MB in the presence of the nanomaterials

The degradation of MB under X-rays was evaluated by following its decrease in absorbance at a wavelength of 664 nm. The MB kinetic plots as a function of absorbed dose are presented in Fig. 3a and b for two different dose rates using an output voltage of 225 kV. The irradiation procedures were carried up to 150 min (i.e 2.5 h) at a dose rate of 8 Gy/min and up to 60 min at a dose rate of 35 Gy/min to achieve a dye degradation of ~90%. Our results indicate a first-order kinetic reaction of the methylene blue decomposition, for which the reaction rate is given by the differential equation (Eq. (1))

$$rate = -\frac{dC}{dt} = k_a C \tag{1}$$

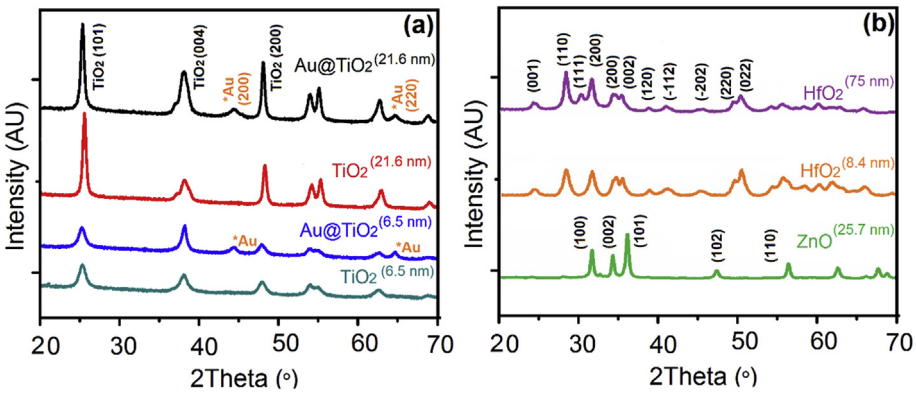

Fig. 1. XRD patterns of **a)** TiO_2 and $Au@TiO_2$ nanocomposites, adapted from (Molina Higgins and Rojas, 2019). **b)** ZnO and HfO_2 NPs.

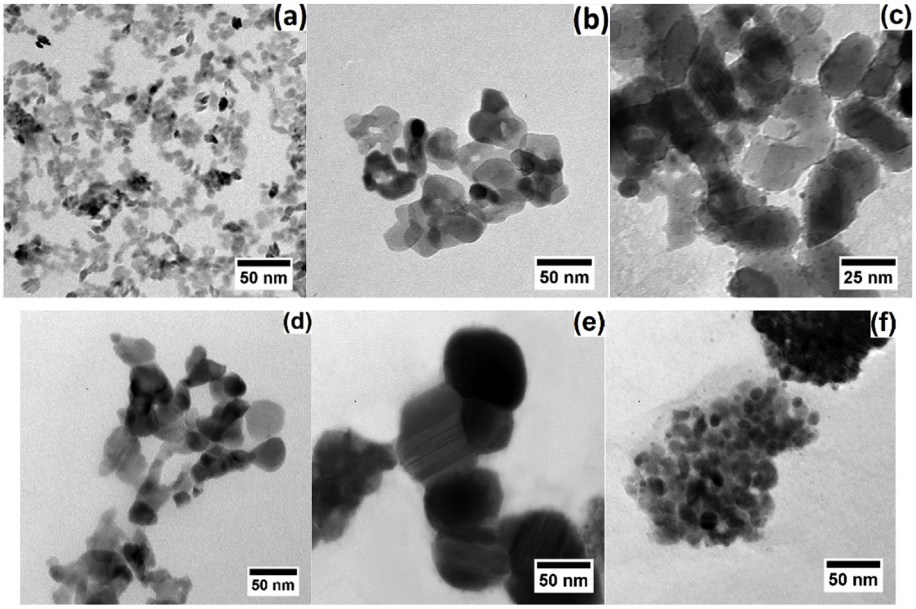

Fig. 2. TEMs of oxides-based for **a)** $TiO_2^{6.5\ nm}$ **b)** $TiO_2^{21.6\ nm}$ **c)** $Au@TiO_2^{21.6\ nm}$ **d)** ZnO **e)** $HfO_2^{75\ nm}$ **f)** $HfO_2^{8.4\ nm}$.

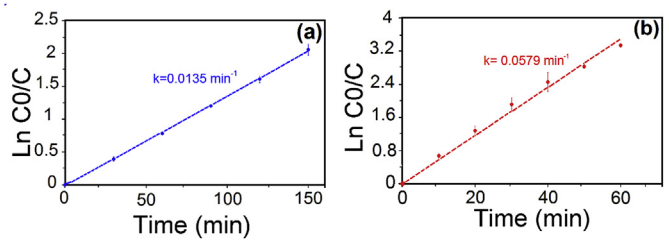

Fig. 3. MB degradation at high irradiation times using a dose rate of **a)** 8 Gy/min **b)** 35 Gy/min.

where C is the MB concentration as a function of time and k_a is the first-order apparent rate constant (El Seoud et al., 2016). The solution to this differential equation gives the trend in which the concentration of the investigated reactant changes with time (El Seoud et al., 2016). The solution concentration of MB as a function of time is given by Eq. (2):

$$\ln\left(\frac{C_0}{C}\right) = -k_a t \tag{2}$$

where C_0 is the initial concentration of MB. In first-order kinetic reactions, the Eq. (2) dictates a linear relationship between Ln (C_0/C) and irradiation time (Singh et al., 2017). The mechanism behind the degradation of MB with X-rays relies on the interaction of high-energy photons with water. Herein, species such as e^-_{aq}, $OH^{\bullet}$, and $O_2^{\bullet -}$ interact with the dye causing gradual degradation. In the absence of particles, the degradation of MB involves reduction and oxidation processes. The reduction process is initiated by the interaction of O_2 molecules with e^-_{aq} producing $O_2^{\bullet -}$ (Yogi et al., 2008). Further interaction of MB with $O_2^{\bullet -}$ causes the transformation of MB into leuco-methylene blue (LMB), which is a double reduced form of the dye (Yogi et al., 2008). The oxidation processes are related to the interaction of MB with $OH^{\bullet}$ producing semi-oxidized species (LaVerne et al., 2005). Other species produced in the radiolysis of water may also interact with the dye and cause its decomposition. In the presence of dissolved oxygen, $H^{\bullet}$ atoms react with O_2 to form hydroperoxyl radicals ($HO_2^{\bullet}$) and cause chemical oxidation of organic molecules (Rauf and Ashraf, 2009). Moreover, species such as e^-_{aq} can react with H_2O_2 to produce $OH^{\bullet}$ and OH^- that contribute to further degradation of the dye (Rauf and Ashraf, 2009). The interaction of $OH^{\bullet}$ with intermediate products continues the degradation to yield simple molecules such as CO_2, SO_4^{2-}, NH_4^+ and NO_3^- (Houas et al., 2001; Twfik et al., 2010). The overall degradation of MB is described by the apparent reaction rate constant k_a for the reaction in Eq. (3). Furthermore, a detailed analysis of the degradation of MB by ionizing radiation at dose rate of 35 Gy/min performed at absorbed doses below 100 Gy, indicates a MB bleaching of 0.85 molecules per 100 eV (G value) which agrees with the range of 0.9–1.1 molecules/100 eV that has been reported in the literature (LaVerne et al., 2005). This analysis is only valid at the beginning of the irradiation process, as the G value decreases with the production of intermediates that may also consume $OH^{\bullet}$ radicals.

$$MB + reactive\ species\ (e^-_{aq},\ OH^{\bullet}) \rightarrow intermediates \rightarrow final\ products \tag{3}$$

It is important to mention that, in all of the experiments, the MB apparent reaction rate constant was evaluated under steady-state radiolysis. In steady-state radiolysis the solutions are irradiated continuously, and the number of reactive species produced in solution will cause consequent dye degradation. Reactions irradiated under steady-state conditions show equilibrium in the rate of species produced and those consumed in solution (Chatterjee et al., 1983; Wren, 2010). Thus, changes in the dye irradiation conditions such as an increase in the dose rate lead to an increase in the concentration of the radiolysis products and a higher degradation rate. The decomposition of MB is characterized by changes in the color of the sample, which can be monitored using spectrophotometry (Subramanian et al., 2016). Under steady-state radiolysis, stable byproducts can also be studied using other tools such as HPLC, FTIR, and NMR (Rauf and Ashraf, 2009).

The plots of kinetic data of MB and its k_a in the presence of each radiocatalyst are shown in Fig. 4a. Furthermore, the results depicted in Fig. 4b shows MB k_a enhancement produced by the presence of the oxides-based nanomaterials. Among the various oxides investigated in this work, TiO_2 was the only oxide that did not exhibit significant radiocatalysis. The k_a of MB in the presence of TiO_2 was ~0.0070 min^{-1}, lower than that in the absence of the particles (0.0149 min^{-1}). In radiosensitization, this phenomenon has been previously evidenced and has been described as anti-enhancement (Guo, 2018). This phenomenon has been defined as the reduction of X-ray effectiveness in the presence of nanomaterials, and anti-enhancement processes are known as ROS decreasing processes (Guo, 2018). There are several pathways that could induce anti-enhancement in nanomaterials. The first one is related with direct scavenging of ROS by the surface of the nanomaterial, the second one is associated with scavenging of ROS by a

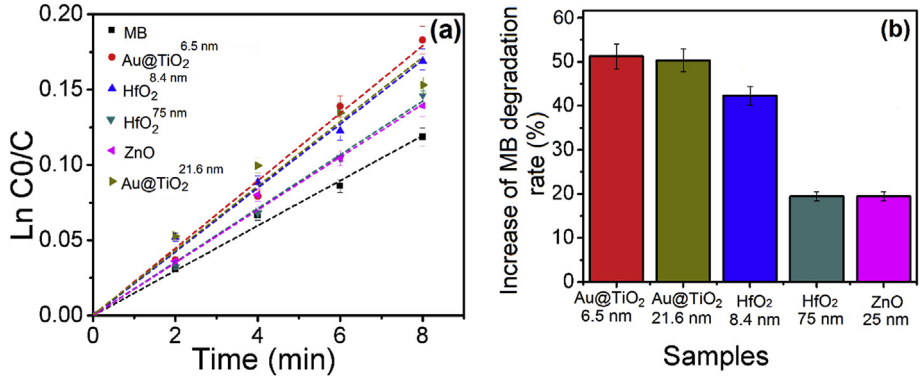

Fig. 4. a) MB apparent reaction rate constants in the presence of oxides-based NPs **b)** Increase of MB apparent reaction rate constant in the presence of the nanomaterial.

chemical group within the ligand, and the third one is related to the direct interaction of ROS with ligands on the nanomaterial's surface (Guo, 2018). In photocatalysis, gold deposition on the surface of titania has shown to modify the electronic band structure and reduce the bandgap of TiO_2, which leads to changes in the recombination rate of carriers within the catalyst (Primo et al., 2011). Measurement of $TiO_2^{6.5\ nm}$ and $TiO_2^{21.6nm}$ bandgap using diffuse reflectance spectroscopy showed values of 3.22 and 3.34 eV, respectively. When Au was deposited on the titania surface, values of 3.27 and 3.08 eV were recorded for $Au@TiO_2^{6.5\ nm}$ and $Au@TiO_2^{21.6\ nm}$, showing than changes in the bandgap of TiO_2 may contribute to an enhanced MB degradation. In our previous work, the addition of TiO_2 in a concentration of 1 mg/ml to a MB solution leads to an increase in the degradation rate under X-rays from 0.067 min^{-1} to 0.073 min^{-1}, indicating that a threshold may exist to cause radiation enhancement (Molina Higgins and Rojas, 2019). As seen in Fig. 4a, when Au was deposited on the TiO_2 surface, the k_a of MB increased by 46.3% and 50.3% for $Au@TiO_2^{21.6\ nm}$ and $Au@TiO_2^{6.5\ nm}$ respectively.

The primary mechanism of interaction of X-rays photons of a 6 MeV bremsstrahlung spectrum with matter is Compton scattering; in this process, photons interact with the electrons in the medium, resulting in a recoil electron and a scattered photon, these interactions are dependent upon the incident energy of the photon (Hoskin, 2012). In aqueous media, the electrons produced in Compton scattering travel short distances before losing their energy and being absorbed by the medium. The scattered photons, on the other hand, travel long distances between each interaction (Hoskin, 2012). For instance, the absorbed dose by the media is due to the gradual energy deposition of both photons and electrons. The presence of the metal oxides increases the absorption of photons energy by the media, leading to a higher absorbed dose that reflects in the MB k_a enhancement. The fractional Photons' energy absorbed by the media that is transferred to the kinetic energy of charged particles is measured by the mass absorption coefficient (Hubell, 1977). The theoretical value of the mass absorption coefficient of water at the endpoint energy of 6 MeV is 0.0181 cm^2/g. On the other hand, the mass absorption coefficients of the nanomaterials used in these experiments are 0.0248 cm^2/g for HfO_2, 0.0198 cm^2/g for ZnO, 0.0189 cm^2/g for $Au@TiO_2$ and, 0.0179 cm^2/g for TiO_2 (Suplee, 2009). Interestingly, while $Au@TiO_2$ has a similar mass absorption coefficient to that of water, this material causes a higher enhancement to the apparent reaction rate constant of MB than that caused by HfO_2, the material with the highest mass absorption coefficient at the similar concentration (i.e. 0.2 mg/ml). This indicates that the radiation enhancement by nanomaterials largely relies on a chemical enhancement. The process of chemical enhancement explains the increased production of ROS through the interaction of Compton electrons and X-rays created by both the nanoparticles and possibly water with adjacent nanoparticles. This phenomenon has also been explained as a result of the interaction of radical intermediates with the nanoparticle's surface rather than increased production of ROS (Guo, 2018, 2019). Thus, chemical enhancement depends heavily on the rate at which intermediate species are created in solution, which depends on the irradiation dose rate and the different pathways of dye degradation upon interaction with either e^-_{aq}, $OH^{\bullet}$, or $O_2^{\bullet -}$ (Guo, 2018). Results reported in a previous study showed that the apparent reaction rate constant of $Au@TiO_2$ irradiated with a dose rate of 3 Gy/min showed a degradation enhancement of 78%, whereas an enhancement of only 65.3% was observed when the dose rate to 35 Gy/min (Molina Higgins and Rojas, 2019). Our results indicate that the radiation enhancement observed is a combination of both photon absorption by the nanoparticles and the ability of the nanomaterials to catalyze chemical compounds at their surface. Overall, the results in this work show that the dose enhancement caused by the presence of the different oxides-based NPs, at a voltage relevant for therapeutic applications, hold great promise of these semiconductors as radiosensitizers.

As shown in Fig. 4b, the addition of ZnO to MB led to the lowest increase in the value of k_a, with an enhancement of 19.5%. Interestingly, from all the evaluated solutions, those containing ZnO had the highest pH with a value of 7.6. In the presence of oxides, MB degradation under UV/visible light has shown to be favored in neutral and alkaline pH (Anju Chanu et al., 2019; Azeez et al., 2018). The reason behind this phenomenon is that MB, being a cationic dye, adsorbs better on the surface of oxides negatively charged, which is promoted at high pH values (Anju Chanu et al., 2019; Tayade et al., 2009). As such, it becomes important to investigate the pzc of the nanomaterials, which provides the pH at which the net charge of the total particle surface becomes zero. This theory explains that at pH values lower than the pzc the surface of the nanomaterial is charged positively, and when the pH is adjusted to values above the pzc, the overall charge surface is negative (Suttiponparnit et al., 2011). In other words, when the pH of the solution is higher than the pzc, the nanomaterial will adsorb the cations from the solution and, when the pH is lower than point of zero charge, the nanomaterial will adsorb anions in solution (Shen, 2016). Table 1, shows a summary of the pH of the solution prior irradiation and the pzc obtained for each support, the obtained values are similar to those

Table 1
pH of the solution and point of zero charge of the radiocatalysts.

Sample	pH of the MB solution	Point of Zero Charge
$TiO_2^{6.5\ nm}$	4.1	6.0
$TiO_2^{21.6\ nm}$	6.1	5.5
$Au@TiO_2^{6.5\ nm}$	4.5	6.2
$Au@TiO_2^{21.6\ nm}$	6.3	5.9
ZnO	7.6	7.6
$HfO_2^{8.4nm}$	6.5	6.7
HfO_2^{75nm}	7.0	7.0

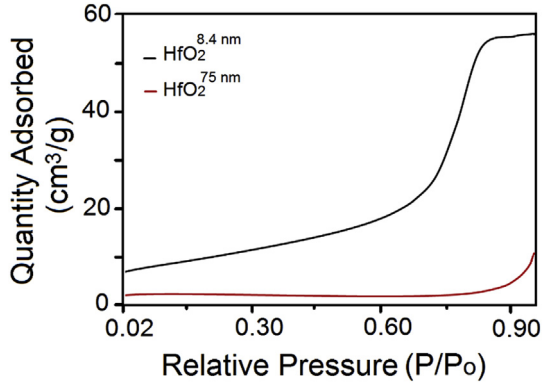

Fig. 5. BET analysis of $HfO_2^{8.4\ nm}$ and $HfO_2^{75\ nm}$.

presented in the literature (Adil et al., 2016; Kosmulski, 2002, 1997). The results showed that $TiO_2^{21.6nm}$ and Au@ $TiO_2^{21.6nm}$ had a pzc higher than the pH of the solution, and therefore a negatively charged surface. Nonetheless, high values for k_a were also found in materials with a pzc lower than the pH of the solution. This may indicate that the degradation of MB takes place mostly in the bulk of the solution by its interaction with reactive species rather than being adsorbed onto the nanoparticles for its subsequent degradation.

An enhancement in the k_a of MB by 19.5% for $HfO_2^{75\ nm}$ and 42.3% for $HfO_2^{8.4\ nm}$ was observed. The high apparent reaction rate constant of MB found in the presence of $HfO_2^{8.4\ nm}$ is due to parameters such as particle size and specific surface area. These parameters have shown to affect the materials' catalytic performance as they control the active sites on the NP surface (Guo, 2018; Jang et al., 2001). The significant difference in the MB apparent reaction rate constant observed between $HfO_2^{8.4\ nm}$ and $HfO_2^{75\ nm}$ catalysts support the fact that smaller particles increase the k_a of the dye. To evaluate the specific surface area of both $HfO_2^{8.4\ nm}$ and HfO_2^{75nm} BET surface area analysis was performed using N_2 gas, and the results are shown in Fig. 5. The isotherm profile of $HfO_2^{8.4\ nm}$ indicates a mixture of type II and Type IV according to IUPAC classification, while that of $HfO_2^{75\ nm}$ resembles a type III classification. The specific surface areas associated with $HfO_2^{8.4\ nm}$ and $HfO_2^{75\ nm}$ were found to be 32.2 m^2/g and 9.5 m^2/g respectively. The relatively higher specific surface area of $HfO_2^{8.4\ nm}$, associated with their small particle size, further justify the higher enhancement in k_a for MB when compared with that using $HfO_2^{75\ nm}$. The influence of the surface area on the radiocatalytic performance of HfO_2 was further studied, and results are shown in Fig. 6. For this purpose, the concentrations of $HfO_2^{8.4\ nm}$ and $HfO_2^{75\ nm}$ were varied to achieve similar values of surface areas of 64.4, 77.3 and 96.6 cm^2. Thus, nanoparticle concentrations in MB were 0.18, 0.24 and 0.3 mg/ml for $HfO_2^{8.4nm}$, and 0.6, 0.8 and 1 mg/ml for $HfO_2^{75\ nm}$. Overall, the results showed that the radiocatalysis of $HfO_2^{8.4\ nm}$ is superior to $HfO_2^{75\ nm}$ at all experimental

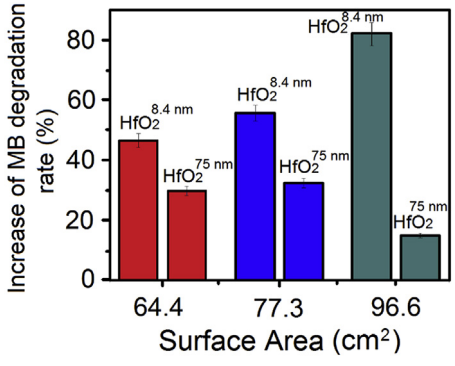

Fig. 6. Increase of MB degradation rate in the presence of $HfO_2^{8.4\ nm}$ and $HfO_2^{75\ nm}$ at different surface areas conditions.

conditions, and they lead to MB degradation enhancement to be directly proportional to their surface area. This may be attributed to the higher probability in smaller particles for charge carriers to diffuse within the material and reach the surface before they annihilate, causing increased catalytic activities. Furthermore, the lower catalytic activity of $HfO_2^{75\ nm}$ could also be associated with the aggregation of the nanoparticles due to the higher concentrations in solution as compared to $HfO_2^{8.4\ nm}$. The hydrodynamic size of the nanoparticles, as measured by Dynamic Light scattering (DLS), was 25 nm and 634 nm for $HfO_2^{8.4\ nm}$ and $HfO_2^{75\ nm}$ at concentrations of 0.2 and 0.6 mg/ml respectively, corresponding to an estimated surface area of 64.4 cm^2. These results confirmed a substantial aggregation of $HfO_2^{75\ nm}$, a feature that could diminish their catallactic activity. As observed in Fig. 6, a change in concentration of $HfO_2^{75\ nm}$ in suspension with MB from 0.6 to 0.8 mg/ml led to a similar MB degradation enhancement of ~30%. Therefore, the mass concentration of HfO_2^{75nm} does not significantly affect MB degradation. Moreover, there is a significant decrease in the MB degradation enhancement at $HfO_2^{75\ nm}$ at a concentration of 1 mg/ml, which could be due to increased aggregation of the particles in suspension and recombination of reactive species at such large concentrations.

The k_a of MB in the presence of nanoparticles, at a concentration of 0.2 mg/ml, and irradiated using a medical LINAC are summarized in Table 2. These results show an enhancement in k_a when metal oxide-based NPs are used as radiocatalysts. Overall, our experiments showed the ability of metal oxides semiconductors to enhance the effectiveness of X-ray irradiation through the mechanism of physical and chemical enhancement. Upon photon activation, holes migrate to the surface of the metal oxides and react with water to produce $OH^{\bullet}$ radicals, whereas electrons will reduce oxygen molecules to produce $O_2^{\bullet-}$. These species will ultimately accelerate dye decomposition (LaVerne et al., 2005). Particularly, low and high energies photons such as UV light and high energy X-rays respectively, favor chemical enhancement of nanomaterials, whereas moderate X-rays energies (50–60 keV) favor physical enhancement (Guo, 2018), a process that is predominant with high Z materials such as Au or HfO_2.

3.3. Discussion of radiocatalysis at different experimental conditions

Direct comparison of the k_a of MB obtained at 8 Gy/min and a 6 MeV LINAC can be drawn with those reported using a commercial irradiator at 225 kV and an absorbed dose rate of 35 Gy/min, pertinent conditions for environmental applications. The k_a of MB in a 225-kV irradiator and 35 Gy/min was ~3.9 times higher than recorded at 6 MeV at a dose rate of 8 Gy/min (see Fig. 3 and Table 2). The k_a of MB was also evaluated at 225 kV, 8 Gy/min, and 2.5 h of irradiation, giving a value of 0.0135 min^{-1} and supporting the fact that MB degradation is a process that is dependent on the dose rate. This is an important feature for the catalytic industry, where pollutant decomposition could be carried out at low voltages and high dose rates. In previous work, the irradiation of MB at a dose rate of 35 Gy/min in the presence of $Au@TiO_2^{6.5\ nm}$ radiocatalysts led to a k_a of 0.110 min^{-1}, corresponding

Table 2
MB apparent reaction rate constants in the presence of oxides-based NPs under X-rays. Standard deviations were obtained from the results of three replicates.

Sample	Endpoint Energy (MeV)	Dose rate (Gy/min)	k_a (min^{-1})	Standard deviation (min^{-1})
MB	6	8	0.0149	0.003
$Au@TiO_2^{21.6\ nm}$	6	8	0.0218	0.004
$Au@TiO_2^{6.5\ nm}$	6	8	0.0224	0.003
$HfO_2^{8.4\ nm}$	6	8	0.0212	0.003
$HfO_2^{75\ nm}$	6	8	0.0182	0.003
ZnO	6	8	0.0178	0.0003

to an enhancement in k_a of 64.2% (Molina Higgins and Rojas, 2019). The degradation of MB in the presence of Au@TiO_2 was also evaluated at a dose rate of 8 Gy/min using a commercial irradiator of 225 kV, in order to compare MB degradation at orthovoltage and megavoltage conditions. The k_a of MB in the presence of Au@$TiO_2^{6.5nm}$ was 0.017 ± 0.001 min^{-1}, and enhancement of 25.9% in k_a was found. At these experimental conditions, a MB degradation of 90.5% was achieved after 2.5 h of irradiation.

The catalytic performance of plain TiO_2 under ionizing radiation has been investigated at a dose rate of 80 Gy/min using a Co-60 irradiator (average $E_{photon} = 1.25$ MeV) (Samet et al., 2018). The results showed that the addition of metals such as copper in the surface of titania increases MB degradation efficiency up to 25%. Moreover, the presence of Cu changes the optical and structural properties of TiO_2 by reducing the bandgap of the semiconductor (Samet et al., 2018). Overall, our work evidenced the performance of various oxides and oxide-based nanomaterials under irradiation with photons of energies applicable to radiotherapy, which is using photons in the megavoltage energy range where Compton scattering is predominant. The degradation of organic molecules with orthovoltage X-rays on the other hand, where the emission of photoelectrons, Auger electrons, characteristic X-rays, is a concept that could be used to enhance pollutant decomposition in water streams.

Radiocatalysis in the field of medicine using nanomaterials such as of TiO_2, ZnO, HfO_2, and Au has been evidenced in the past for in-vivo and in-vitro testing as radiosensitizers (Generalov et al., 2015; Maggiorella et al., 2012; McGinnity et al., 2016; Youkhana et al., 2017). A significant radiation enhancement has been observed with TiO_2 in biological scenarios. The authors used a collimated and filtered beam of X-rays at a maximum voltage of 80 kV and an enhancement of 77% and 70% was observed in DU145 and in HaCaT cells respectively; DU145 are human prostate cancer and HaCaT are human skin cell lines. In the same work, the radiation dose enhancement of TiO_2 was tested at the megavoltage range (6 MV) using chemical dosimetry. A dose rate enhancement factor of 1.04 was achieved, which is equivalent to a radiation dose enhancement of 4% (Youkhana et al., 2017). These results are in agreement with the TiO_2 radiosensitization in the present work, where negligible to none radiation enhancement was observed. On the other hand, ZnO-silica NPs have been studied as a radiosensitizer in DU145 cells irradiated with 200 kVp X-rays. The dose enhancement varied from 10% at a nominal absorbed dose of 2 Gy up to 56% when the nominal absorbed dose increased to 10 Gy (Generalov et al., 2015). Lastly, HfO_2-based NPs are currently in clinical trials under the commercial name Nanobiotix. In vitro experiments at the megavoltage range showed a tumor growth inhibition of 82% at an absorbed dose of 15 Gy. A similar enhancement value was found in this work when HfO_2 in a concentration of 0.3 mg/ml was added to MB. Their results also show that the tumor growth inhibition using HfO_2 was 72% for radiation alone (Maggiorella et al., 2012). Moreover, Monte Carlo simulations calculated a dose enhancement of 15% while using a simulated 6 MeV photon beam (Maggiorella et al., 2012). The pioneer experiments exploring nanomaterial's radiosensitization were conducted using Au NPs as radiosensitizers and presented by Hainfeld et al., in 2004. The authors injected 2 nm NPs Au NPs in mice mammary carcinomas (Hainfeld et al., 2004). Irradiation was carried out with 250 kVp X-rays and an absorbed dose of 30 Gy (Hainfeld et al., 2004). Their results showed an increase in the one-year survival of mice from 20% to 86% using Au NPs at a concentration of 2.7 g of Au/kg body weight (Hainfeld et al., 2004). Our work investigated the radiosensitization of different metal oxides-based NPs using chemical dosimetry, at equivalent concentrations within the organic probe and irradiation conditions of interest to radiation therapy. Our results evidenced the successful performance of such materials and set a baseline to assess radiosensitivity in future experiments in biological scenarios.

4. Conclusions

Metal oxide and oxide-based NPs were successfully tested as radiocatalysts. The higher MB apparent reaction rate constants found in the presence of the nanomaterials was due to the increase in the production of ROS generated from the interaction of X-rays with the particles. Results using a medical LINAC, that provides photons with energies relevant to radiation therapy, indicated that metal oxide composed of high Z elements such as Hf and Au, showed superior k_a of MB when compared with metal oxides of low Z elements. Furthermore, HfO_2 NPs with a small mean particle size of 8.4 nm led to a higher k_a of MB when compared to larger particles (~75 nm) by a factor of 2.2 at a concentration of 0.2 mg/ml. Analysis of different HfO_2 concentrations in MB solutions at similar surface areas showed that $HfO_2^{8.4nm}$ has a higher catalytic activity than HfO_2^{75nm} at all experimental conditions. The deposition of Au onto the TiO_2 increased its performance for the degradation of MB. This is due to the ability of Au to reduce electron-hole pair recombination in TiO_2, and thus contribute to the increase in ROS production, and the photoemissions released by Au upon X-ray irradiation. The results presented throughout this work demonstrates the feasibility of metal oxides as radiocatalyst for a variety of voltages relevant to radiation therapy. This concept can be further explored for water remediation, in a catalytic process carried at atmospheric temperature and pressure, without the need for toxic bleaching agents.

CRediT authorship contribution statement

M. Molina Higgins: Conceptualization, Methodology, Validation, Formal analysis, Investigation, Data curation, Writing - original draft, Writing - review & editing, Visualization. **A. Banu:** Investigation, Resources, Writing - review & editing. **S. Pendleton:** Investigation, Resources, Writing - review & editing. **J.V. Rojas:** Conceptualization, Methodology, Formal analysis, Investigation, Resources, Writing - review & editing, Supervision, Funding acquisition.

Declaration of competing interest

The authors confirm that there are no conflicts to declare.

Acknowledgments

The Authors acknowledge the support given by the Department of Mechanical and Nuclear Engineering from Virginia Commonwealth University (VCU), the VCU Presidential Research Quest Fund (PeRQ), and the Nuclear Regulatory Commission under the federal grant award number HQ-84-14-G-0051 Faculty Development Program in Radiation Defection and Health Physics. More importantly, the authors wish to thank the Madison accelerator laboratory (MAL) at JMU.

References

Adil, M., Zaid, H.M., Chuan, L.K., Latiff, N.R.A., 2016. Effect of dispersion stability on electrorheology of water-based ZnO nanofluids. Energy Fuels 30, 6169–6177. https://doi.org/10.1021/acs.energyfuels.6b01116.

Anju Chanu, L., Joychandra Singh, W., Jugeshwar Singh, K., Nomita Devi, K., 2019. Effect of operational parameters on the photocatalytic degradation of Methylene blue dye solution using manganese doped ZnO nanoparticles. Results Phys 12, 1230–1237. https://doi.org/10.1016/j.rinp.2018.12.089.

Appleby, A., Schwarz, H.A., 1969. Radical and molecular yields in water irradiated by .gamma.-rays and heavy ions. J. Phys. Chem. 73, 1937–1941. https://doi.org/10.1021/j100726a048.

Azeez, F., Al-Hetlani, E., Arafa, M., Abdelmonem, Y., Nazeer, A.A., Amin, M.O., Madkour, M., 2018. The effect of surface charge on photocatalytic degradation of methylene blue dye using chargeable titania nanoparticles. Sci. Rep. 8, 1–9. https://doi.org/10.1038/s41598-018-25673-5.

Banerjee, B., 2017. Recent developments on nano-ZnO catalyzed synthesis of bioactive heterocycles. J. Nanostructure Chem. 7, 389–413. https://doi.org/10.1007/s40097-017-0247-0.

Beek, W.J.E., Wienk, M.M., Janssen, R.A.J., 2004. Efficient hybrid solar cells from zinc oxide nanoparticles and a conjugated polymer. Adv. Mater. 16, 1009–1013. https://doi.org/10.1002/adma.200306659.

Belloni, J., Mostafavi, M., Remita, H., Marignier, J.-L., Delcourt, M.-O., 1998. Radiation-induced synthesis of mono- and multi-metallic clusters and nanocolloids. New J. Chem. 22, 1239–1255. https://doi.org/10.1039/A801445K.

Chatterjee, A., Magee, J.L., Dey, S.K., 1983. The role of homogeneous reactions in the radiolysis of water. Radiat. Res. 96, 1–19. https://doi.org/10.2307/3576159.

Chen, H, Wang, L, 2014. Nanostructure sensitization of transition metal oxides for visible-light photocatalysis. Beilstein J. Nanotechnol. 5, 696–710. https://doi.org/10.3762/bjnano.5.82.

Cheng, M., Zeng, G., Huang, D., Lai, C., Xu, P., Zhang, C., Liu, Y., 2016. Hydroxyl radicals based advanced oxidation processes (AOPs) for remediation of soils contaminated with organic compounds: a review. Chem. Eng. J. 284, 582–598. https://doi.org/10.1016/j.cej.2015.09.001.

Clifford, D.M., Castano, C.E., Rojas, J.V., 2017. Supported transition metal nanomaterials: nanocomposites synthesized by ionizing radiation. Radiat. Phys. Chem. 132, 52–64. https://doi.org/10.1016/j.radphyschem.2016.12.001.

Čubová, K., Čuba, V., 2019. Synthesis of inorganic nanoparticles by ionizing radiation – a review. Radiat. Phys. Chem. 158, 153–164. https://doi.org/10.1016/j.radphyschem.2019.02.022.

Djurišić, A.B., Ng, A.M.C., Chen, X.Y., 2010. ZnO nanostructures for optoelectronics: material properties and device applications. Prog. Quant. Electron. 34, 191–259. https://doi.org/10.1016/j.pquantelec.2010.04.001.

El Seoud, O.A., Baader, W.J., Bastos, E.L., 2016. Practical chemical kinetics in solution. In: Wang, Z. (Ed.), Encyclopedia of Physical Organic Chemistry, 5 Volume Set. John Wiley & Sons, Inc., Hoboken, NJ, USA, pp. 1–68. https://doi.org/10.1002/9781118468586.epoc1012.

Gao, D., Zhang, Z., Fu, J., Xu, Y., Qi, J., Xue, D., 2009. Room temperature ferromagnetism of pure ZnO nanoparticles. J. Appl. Phys. 105, 113928. https://doi.org/10.1063/1.3143103.

Generalov, R., Kuan, W.B., Chen, W., Kristensen, S., Juzenas, P., 2015. Radiosensitizing effect of zinc oxide and silica nanocomposites on cancer cells. Colloids Surf. B Biointerfaces 129, 79–86. https://doi.org/10.1016/j.colsurfb.2015.03.026.

Zacheis, George Adam, Gray, Kimberly A., Kamat, Prashant V., 1999. Radiation-Induced Catalysis on Oxide Surfaces: Degradation of Hexachlorobenzene on γ-Irradiated Alumina Nanoparticles. WWW Document. https://doi.org/10.1021/jp990211u.

Guo, T., 2019. Physical, chemical and biological enhancement in X-ray nanochemistry. Phys. Chem. Chem. Phys. 21, 15917–15931. https://doi.org/10.1039/C9CP03024G.

Guo, T., 2018. X-ray Nanochemistry: Concepts and Development. Springer Science +Business Media, New York, NY.

Hainfeld, J.F., Slatkin, D.N., Smilowitz, H.M., 2004. The use of gold nanoparticles to enhance radiotherapy in mice. Phys. Med. Biol. 49, N309–N315.

Hamill, W., 1969. Model for the radiolysis of water - the journal of physical chemistry (ACS publications). J. Phys. Chem. 73, 1341–1347.

Her, S., Jaffray, D.A., Allen, C., 2017. Gold nanoparticles for applications in cancer radiotherapy: mechanisms and recent advancements. Adv. Drug Deliv. Rev., Radiotherapy for cancer: present and future 109, 84–101. https://doi.org/10.1016/j.addr.2015.12.012.

Hoertz, P., Damaris, M-A., Gupta, V., Norton, C., Doorn, S., Ennis, T., 2013. Photocatalytic and radiocatalytic nanomaterials for the degradation of organicspecies. Radiat. Phys. Chem. 54, 51–58. https://doi.org/10.1016/j.radphyschem.2012.06.045.

Hoskin, P., 2012. Basic physics. In: External Beam Therapy. Oxford University Press, pp. 6–25.

Houas, A., Lachheb, H., Ksibi, M., Elaloui, E., Guillard, C., Herrmann, J.-M., 2001. Photocatalytic degradation pathway of methylene blue in water. Appl. Catal. B Environ. 31, 145–157. https://doi.org/10.1016/S0926-3373(00)00276-9.

Hubell, J.H., 1977. Photon mass attenuation and mass energy-absorption coefficients for H, C, N, O, Ar, and seven mixtures from 0.1 keV to 20 MeV. Radiat. Res. 70, 58–81. https://doi.org/10.2307/3574732.

Jang, H.D., Kim, S.-K., Kim, S.-J., 2001. Effect of particle size and phase composition of titanium dioxide nanoparticles on the photocatalytic properties. J. Nanoparticle Res. 3, 141–147. https://doi.org/10.1023/A:1017948330363.

Jayaraman, V., Bhavesh, G., Chinnathambi, S., Ganesan, S., Aruna, P., 2014. Synthesis and Characterization of Hafnium Oxide Nanoparticles for Bio-Safety. [WWW Document]. https://doi.org/10.1166/mex.2014.1190.

Kosmulski, M., 2002. The significance of the difference in the point of zero charge between rutile and anatase. Adv. Colloid Interface Sci. 99, 255–264. https://doi.org/10.1016/S0001-8686(02)00080-5.

Kosmulski, M., 1997. Attempt to determine pristine points of zero charge of Nb2O5, Ta2O5, and HfO2. Langmuir 13, 6315–6320. https://doi.org/10.1021/la970469g.

Kotagiri, N., Sudlow, G.P., Akers, W.J., Achilefu, S., 2015. Breaking the depth dependency of phototherapy with cerenkov radiation and low radiance responsive nanophotosensitizers. Nat. Nanotechnol. 10, 370–379. https://doi.org/10.1038/nnano.2015.17.

Kovács, A., Wojnárovits, L., Kurucz, C., Al-Sheikhly, M., McLaughlin, W.L., 1998. Large-scale dosimetry using dilute methylene blue dye in aqueous solution. In: Radiat. Phys. Chem., Proceedings of the 10th International Meeting on Radiation Processing, vol. 52. pp. 539–542. https://doi.org/10.1016/S0969-806X(98)00091-7.

Kuncic, Z., Lacombe, S., 2018. Nanoparticle radio-enhancement: principles, progress and application to cancer treatment. Phys. Med. Biol. 63, 02TR01. https://doi.org/10.1088/1361-6560/aa99ce.

LaVerne, J.A., 2000. OH radicals and oxidizing products in the gamma radiolysis of water. Radiat. Res. 153, 196–200. https://doi.org/10.1667/0033-7587(2000)153[0196:ORAOPI]2.0.CO;2.

LaVerne, J.A., Tandon, L., Knippel, B.C., Montoya, V.M., 2005. Heavy ion radiolysis of methylene blue. Radiat. Phys. Chem., Christiane Ferradini Memorial Issue 72, 143–147. https://doi.org/10.1016/j.radphyschem.2004.09.010.

Maggiorella, L., Barouch, G., Devaux, C., Pottier, A., Deutsch, E., Bourhis, J., Borghi, E., Levy, L., 2012. Nanoscale radiotherapy with hafnium oxide nanoparticles. Future Oncol. 8, 1167–1181. https://doi.org/10.2217/fon.12.96.

McGinnity, T.L., Dominguez, O., Curtis, T.E., Nallathamby, P.D., Hoffman, A.J., Roeder, R.K., 2016. Hafnia (HfO2) nanoparticles as an X-ray contrast agent and mid-infrared biosensor. Nanoscale 8, 13627–13637. https://doi.org/10.1039/C6NR03217F.

Mesbahi, A., 2010. A review on gold nanoparticles radiosensitization effect in radiation therapy of cancer. Rep. Practical Oncol. Radiother. 15, 176–180. https://doi.org/10.1016/j.rpor.2010.09.001.

Molina Higgins, M.C., Clifford, D.M., Rojas, J.V., 2018. Au@TiO2 nanocomposites synthesized by X-ray radiolysis as potential radiosensitizers. Appl. Surf. Sci. 427, 702–710. https://doi.org/10.1016/j.apsusc.2017.08.094.

Molina Higgins, M.C., Rojas, J.V., 2019. X-ray radiation enhancement of gold- TiO2 nanocomposites. Appl. Surf. Sci. 480, 1147–1155. https://doi.org/10.1016/j.apsusc.2019.02.234.

Nakata, K., Fujishima, A., 2012. TiO2 photocatalysis: design and applications. J. Photochem. Photobiol. C Photochem. Rev. 13, 169–189. https://doi.org/10.1016/j.jphotochemrev.2012.06.001.

Niu, Z., Li, Y., 2014. Removal and utilization of capping agents in nanocatalysis. Chem. Mater. 26, 72–83. https://doi.org/10.1021/cm4022479.

Primo, A., Corma, A., García, H., 2011. Titania supported gold nanoparticles as photocatalyst. Phys. Chem. Chem. Phys. PCCP 13, 886–910. https://doi.org/10.1039/c0cp00917b.

Rajaee, A., Zhao, L., Wang, S., Wang, D., Liu, Y., Wang, J., Ying, K., 2019. Multifunction bismuth gadolinium oxide nanoparticles as radiosensitizer in radiation therapy and imaging. Phys. Med. Biol. https://doi.org/10.1088/1361-6560/ab2154.

Rauf, M.A., Ashraf, S.S., 2009. Radiation induced degradation of dyes—an overview. J. Hazard Mater. 166, 6–16. https://doi.org/10.1016/j.jhazmat.2008.11.043.

Sahu, S.P., Cates, E.L., 2017. X-ray Radiocatalytic Activity and Mechanisms of Bismuth Complex Oxides. [WWW Document]. https://doi.org/10.1021/acs.jpcc.7b00776.

Samet, L., March, K., Stephan, O., Brun, N., Hosni, F., Bessousa, F., Benasseur, J., Chtourou, R., 2018. Radiocatalytic Cu-incorporated TiO2 nano-particles for the degradation of organic species under gamma irradiation. J. Alloys Compd. 743, 175–186. https://doi.org/10.1016/j.jallcom.2018.02.001.

Shen, X., 2016. 10 - molecularly imprinted photocatalysts. In: Li, S., Cao, S., Piletsky, S.A., Turner, A.P.F. (Eds.), Molecularly Imprinted Catalysts. Elsevier, Amsterdam, pp. 211–228. https://doi.org/10.1016/B978-0-12-801301-4.00010-4.

Singh, J., Chang, Y.-Y., Koduru, J.R., Yang, J.-K., 2017. Potential degradation of methylene blue (MB) by nano-metallic particles: a kinetic study and possible mechanism of MB degradation. Environ. Eng. Res. 23, 1–9. https://doi.org/10.4491/eer.2016.158.

Stafford, U., Gray, K.A., Kamat, P.V., 1994. Radiolytic and TiO2-assisted photocatalytic degradation of 4-chlorophenol. A comparative study. J. Phys. Chem. 98, 6343–6351. https://doi.org/10.1021/j100076a019.

Subramanian, V., Joseph, J.M., Subramanian, H., Noël, J.J., Guzonas, D.A., Wren, J.C., 2016. Steady-state radiolysis of supercritical water: model predictions and validation. J. Nucl. Eng. Radiat. Sci. 2. https://doi.org/10.1115/1.4031199.

Suplee, C., 2009. X-Ray Mass Attenuation Coefficients. [WWW Document]. NIST. URL. https://www.nist.gov/pml/x-ray-mass-attenuation-coefficients accessed 2.1.19.

Suttiponparnit, K., Jiang, J., Sahu, M., Suvachittanont, S., Charinpanitkul, T., Biswas, P., 2011. Role of surface area, primary particle size, and crystal phase on titanium dioxide nanoparticle dispersion properties. Nanoscale Res. Lett. 6https://doi.org/10.1007/s11671-010-9772-1. 27–27.

Tayade, R.J., Natarajan, T.S., Bajaj, H.C., 2009. Photocatalytic degradation of methylene blue dye using ultraviolet light emitting diodes. Ind. Eng. Chem. Res. 48, 10262–10267. https://doi.org/10.1021/ie9012437.

Tourneau, C.L., Calugaru, V., Thariat, J.O., Florescu, C., Mirabel, X., Jegoux, F., Jouffroy, T., Rodriguez, J., Hoffmann, C., Dodger, B., Garcia, V.M., Dimitriu, M., Levy, L., Calvo, E., 2018. Hafnium oxide nanoparticles as a promising emergent treatment for head and neck cancer. Int. J. Radiat. Oncol. Biol. Phys. 100, 1377. https://doi.org/10.1016/j.ijrobp.2017.12.180.

Twfik, A.F., Baraka, A.A., El-Sayed, M.A., Omar, A.M., 2010. GAMMA-RAY induced catalytic degradation OF methylene blue IN aqueous suspension OF titania. Int. Conf. Chem. Environ. Eng. 5, 1–15.

Védrine, J.C., 2017. Heterogeneous catalysis on metal oxides. Catalysts 7, 341. https://doi.org/10.3390/catal7110341.

Wan, Y., Zhou, X., 2017. Formation mechanism of hafnium oxide nanoparticles by a hydrothermal route. RSC Adv. 7, 7763–7773. https://doi.org/10.1039/C6RA26663K.

Wang, H., Mu, X., He, H., Zhang, X.-D., 2018. Cancer radiosensitizers. Trends Pharmacol. Sci. 39, 24–48. https://doi.org/10.1016/j.tips.2017.11.003.

Wren, J.C., 2010. Steady-state radiolysis: effects of dissolved additives. In: Nuclear Energy and the Environment, ACS Symposium Series. American Chemical Society, pp. 271–295. https://doi.org/10.1021/bk-2010-1046.ch022.

Yin, Z.F., Wu, L., Yang, H.G., Su, Y.H., 2013. Recent progress in biomedical applications of titanium dioxide. Phys. Chem. Chem. Phys. 15, 4844–4858. https://doi.org/10.1039/C3CP43938K.

Yogi, C., Kojima, K., Takai, T., Wada, N., 2008. Photocatalytic degradation of methylene blue by Au-deposited TiO2 film under UV irradiation. J. Mater. Sci. 44, 821. https://doi.org/10.1007/s10853-008-3151-7.

Youkhana, E.Q., Feltis, B., Blencowe, A., Geso, M., 2017. Titanium dioxide nanoparticles as radiosensitisers: an in vitro and phantom-based study. Int. J. Med. Sci. 14, 602–614. https://doi.org/10.7150/ijms.19058.

Zhou, R., Wang, H., Yang, Y., Zhang, C., Dong, X., Du, J., Yan, L., Zhang, G., Gu, Z., Zhao, Y., 2019. Tumor microenvironment-manipulated radiocatalytic sensitizer based on bismuth heteropolytungstate for radiotherapy enhancement. Biomaterials 189, 11–22. https://doi.org/10.1016/j.biomaterials.2018.10.016.